INTERNATIONAL JOURNAL FOR NUMERICAL METHODS IN ENGINEERING
Int. J. Numer. Meth. Engng 2013; **95**:529–540
Published online 25 June 2013 in Wiley Online Library (wileyonlinelibrary.com). DOI: 10.1002/nme.4537

Energy conservative property of impulse-based methods for collision resolution

XH Tang, A Paluszny*,† and R. W. Zimmerman

Department of Earth Science and Engineering, Imperial College , London, UK

SUMMARY

Physical accuracy, numerical stability, and computational speed are critical factors in the simulation of collisions. The impulse-based method models collisions in a system of rigid bodies in a relatively reliable and fast manner. In the present paper, evidence is presented for the energy-conserving and momentum-conserving properties of the method. Two different impulse-based approaches are validated using numerical tests. A necessary condition is proposed for the impulse-based method to be energy conservative. Results indicate that the impulse-based method for collision simulation, which satisfies the proposed condition, is energy conservative. Copyright © 2013 John Wiley & Sons, Ltd.

Received 22 March 2012; Revised 7 March 2013; Accepted 14 May 2013

KEY WORDS: Impulse-based method; energy conservation; linear momentum conservation; collision resolution

1. INTRODUCTION

The simulation of collision-driven interactions in a multi-body system is instrumental in modeling scenarios for the prediction and control of industrial processes and adds to the understanding of their controlling mechanisms. Often involving hundreds of thousands to millions of interacting bodies, simulations must constantly weigh numerical stability, physical accuracy, and computational speed, if they are to become industrial tools. This trade-off is especially critical in the simulation of rock fragmentation for mining engineering [1, 2], and for tumble mills in agriculture [3], for which geometric representation is believed to play a decisive role in the interaction behavior. The main methods proposed to simulate contacts in a rigid body system include analytic [4], penalty [5], and impulse-based methods [6, 7].

The penalty method [8, 9] transforms constrained optimization problems into a set of non-constrained optimization problems by iteratively computing a proper penalty parameter that enforces collisions as non-penetration [10, 11]. The penalty method is simple and is able to simulate the propagation of impact-induced stress waves within deformable colliding bodies [12]. However, the penalty method suffers from several drawbacks. First, it requires knowledge of the value of normal and tangential stiffness of a force-spring system, which is difficult to determine and its estimation is mainly on the basis of experience [13, 14]. Second, if the bodies collide with relative high velocity, large overlap maybe be detected, which leads to large forces and instability in simulation. As a result, a somewhat arbitrary damping parameter is used to cause energy dissipation and remain stable [15, 16]. To guarantee energy conservation, the midpoint integration rule combined with the Lagrange multiplier method [17] and penalty regularization of contact rates [18, 19] have been proposed. Third, the penalty method relies on the expensive and geometrically complex computation

*Correspondence to: A Paluszny, Department of Earth Science and Engineering, Imperial College, London, UK.
†E-mail: apaluszn@imperial.ac.uk

Copyright © 2013 John Wiley & Sons, Ltd.

of penetration distances, volumes, and surfaces over intersection of two colliding bodies to compute the damping condition [20].

In engineering, the penalty method is widely used in the context of the discrete element method (DEM) [21, 22], smoothed particle hydrodynamics (SPH) [23, 24], material point method, and discontinuous deformation analysis (DDA) [25]. These three methods are able to simulate the collision and contact between two bodies, as well as being able to simulate the deformation and fracturing of deformable bodies. The collision resolution of the previous methods is based on the a posteriori penalization of mesh penetration. DEM assembles a set of tetrahedra [26, 27] or sphere-conglomerates [1, 28] in three dimensions. SPH [29] and material point method [30, 31] are both point-based methods, often applied to simulate explosions and problems involving large deformations. Both apply point-to-point contact detection associated with difficulty in determining direction of the contact force vector [32]. DDA solves for the stresses, displacements, and contacts of bodies by minimizing the potential energy and represents strain energy from the contact force as a function of penetration. Solving all the constraints in a system of linear equations renders DDA to be extremely time consuming as compared with the impulse method.

Analytical methods compute contact forces by expressing the system as a linear complementary problem [33]. Analytical methods do not require the determination of a penalty parameter and do not require the damping parameter to remain stable. One drawback of analytical methods is to consider the influence of friction. This system becomes complex when dynamic friction is added, as the defining matrix becomes non-symmetric and non-positive definite, for example, [16]. Furthermore, when static friction is considered, the constraints of the two tangent directions at the contact point become nonlinear, and the problem becomes a nonlinear complementarity problem. An alternative method is the Lagrange multiplier method, which does not need to calibrate the penalty parameter and damping parameter and is able to exactly implement the boundary constraints. However, the Lagrange-multiplier method introduces extra unknowns, and furthermore is only available for bilateral constraints, such as joint constraint, and lacks the ability to solve unilateral constraints [16].

The impulse-based method efficiently and accurately models high-frequency collisions of complex non-convex shapes based on sequentially enforcing non-penetration constraints [34–36]. In contrast to analytical methods and Lagrange-based methods, no extra unknowns are added, and the sliding and static frictions are both easy to be applied. Unlike *a posteriori* penalty methods, which compute explicit constraint forces at contact points, it does not rely on arbitrary penetration parameters and damping parameters that define repulsion as a function of penetration. Instead, it predicts collisions as a function of impact between proximal bodies and does not need to calibrate the value of penetration parameter and damping parameters. Third, the impulse-based method does not require full geometric intersection checks during the dynamics simulation; therefore, the fast Lin–Canny algorithm based on non-penetration algorithm [37, 38] is able to be used to identify collision candidates. Fourth, each collision is handled locally, making the method well suited for parallelisation. Last, with the impulse-based method, all types of contact, including sliding and rolling, are modeled within a single formulation.

Recently, a combined impulse-based method and finite element method (IFEM) was applied to simulate the rock fragmentation in block caving engineering [39]. As opposed to DEM, in IFEM, colliding bodies are not represented as a conglomeration of primitive shapes; instead, their geometry is represented using solid modelling techniques. This allows for continuum-mechanics-based fracture propagation analysis to be carried out within each of the colliding bodies. In addition, as compared with DEM, it does not require calibration of micro-to-macro material properties, avoiding artificial deformation effects of particle shape, size, and arrangement [40]. Unlike SPH, IFEM relies on the finite element method to satisfy the constant and linear consistency conditions on free boundaries and to define material interfaces [41].

The analysis of energy dissipation among multiple collisions is a critical issue in engineering, such as the design of comminution device [42–44]. In the present work, the physical accuracy of the impulse-based method is validated in the context of energy and momentum conservation. Energy and momentum for the frictionless and perfect elastic collisions conservation is a basic requirement for a numerical method, which is able to ensure that energy loss in simulation is caused by numerical error. Moreover, a necessary condition for an impulse-based method to be energy

Copyright © 2013 John Wiley & Sons, Ltd.

DOI: 10.1002/nme

conservative is proposed. The present work examines different proposals available in the literature regarding the resolution of collisions using this approach, namely, those proposed by Hahn [34] and Guendelman [7]. Numerical experiments (described below) indicate that Guendelman's approach is energy conservative.

2. IMPULSE-BASED METHOD

Hahn [34] was the first to apply the impulse-momentum form of Newton's second law to compute collision response of multi-body systems [45]. Using this approach, collisions are modeled sequentially and do not require the computation of penetration depth, area, or volume between the interacting bodies. Collision time is assumed to be of infinitesimal duration; therefore, during the collision, the positions of the bodies are treated as constant. Schmitt *et al.* [35] proved that impulse-based solutions for collision converge toward the exact solution of the dynamics problem as the timestep is reduced. This section introduces the impulse-based approaches proposed by Hahn [34] and Guendelman [7].

In a two-body system (see Figure 1), where a body b_i collides with another, b_j, their velocities at the contact point can be expressed as

$$\mathbf{u}_i = \mathbf{v}_i + \boldsymbol{\omega}_i \times \mathbf{r}_i \tag{1}$$

where $\mathbf{r}_i = \left\{r_i^x, r_i^y, r_i^z\right\}^{\mathrm{T}}$ is the vector from the center of the mass of body i to the contact point, $\mathbf{u}_i = \left\{u_i^x, u_i^y, u_i^z\right\}^{\mathrm{T}}$ is the velocity at the contact point, $\mathbf{v}_i$ is the linear velocity of the center of mass, and $\boldsymbol{\omega}_i$ is the angular velocity. At a collision, the relative velocity at the contact point, $\mathbf{u} = \left\{u_x, u_y, u_z\right\}^{\mathrm{T}}$, is defined as

$$\mathbf{u} = \mathbf{u}_j - \mathbf{u}_i \tag{2}$$

The change of velocity caused by a collision during the phases of compression and restitution can be represented by [46]

$$\mathbf{u}_i^f = -e\mathbf{u}_i^b \tag{3}$$

where e is the coefficient of restitution [47]; $e = 0$ for perfectly plastic collisions, and $e = 1$ for perfectly elastic collisions. The subscripts b and f refer to the states before and after collision, respectively. The impulse-based method relies on the accurate computation of the time of contact between objects. The Lin–Canny algorithm [37, 38], a fast search of the closest features among

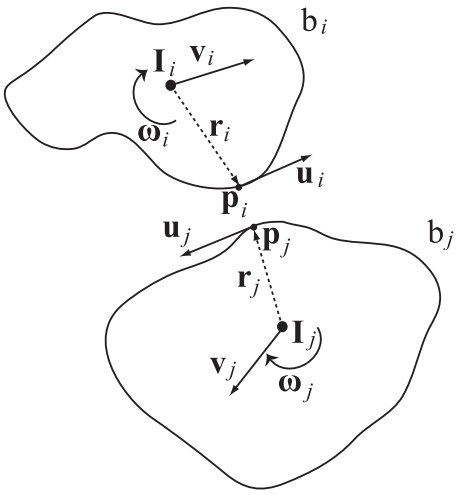


Figure 1. Collision of two bodies b_i and b_j.

Copyright © 2013 John Wiley & Sons, Ltd.

DOI: 10.1002/nme

convex polyhedra, is used to identify collision candidates. A pair of impulses of opposite signs $\mathbf{p}_i = -\mathbf{p} = \mathbf{p}$ are applied directly before collision to model the expected response due to impact and avoid penetration. The applied impulse effectively changes the velocities of the bodies and avoids penetration.

The impulse vector is defined by contributions of the linear and angular velocities of the colliding bodies,

$$\mathbf{p}_i = m_i \triangle \mathbf{v}_i \tag{4}$$

$$\mathbf{r}_i \times \mathbf{p}_i = \mathbf{I}_i \triangle \boldsymbol{\omega}_i \tag{5}$$

where $\mathbf{I}_i$ is the inertia tensor, computed here using an explicit exact expression [48]. The change of relative velocity at a contact point can be expressed as

$$\triangle \mathbf{u} = \mathbf{u}_f - \mathbf{u}_b \tag{6}$$

where $\mathbf{u}_b$ and $\mathbf{u}_f$ are the relative velocities at the contact point before and after collision, respectively.

A local coordinate system $(\mathbf{t}, \mathbf{n}, \mathbf{r})$ is defined in terms of the normal and tangential components of the collision (see Figure 1)

$$\mathbf{r} = \frac{\mathbf{n} \times \mathbf{u}_b}{|\mathbf{u}_b|} \tag{7}$$

$$\mathbf{t} = \mathbf{n} \times \mathbf{r} \tag{8}$$

where $\mathbf{n}$ is the normal direction of collision, and $\mathbf{t}$ and $\mathbf{r}$ are the two tangential directions at the point of impact. The relative velocity and impulse occur on the plane defined by $\mathbf{n}$ and $\mathbf{t}$. Subsequently, the impulse can be decomposed into two orthogonal directions

$$\mathbf{p} = \mathbf{p}_n + \mathbf{p}_t \tag{9}$$

where $\mathbf{p}_n$, normal impulse, and $\mathbf{p}_t$, tangential impulse, are defined as

$$\mathbf{p}_n = (\mathbf{p} \cdot \mathbf{n})\mathbf{n} \tag{10}$$

$$\mathbf{p}_t = \mathbf{p} - \mathbf{p}_n \tag{11}$$

The resolution of the collision can be formulated in terms of this local coordinate system, as follows:

$$\begin{cases} \tilde{\mathbf{u}}_b = \mathbf{L}\mathbf{u}_b \\ \tilde{\mathbf{u}}_f = \mathbf{L}\mathbf{u}_f \\ \tilde{\mathbf{p}} = \mathbf{L}\mathbf{p} \end{cases} \tag{12}$$

where $\tilde{\mathbf{u}}_b = \left\{\tilde{u}_t^b, \tilde{u}_n^b, \tilde{u}_r^b\right\}$ and $\tilde{\mathbf{u}}_f = \left\{\tilde{u}_t^f, \tilde{u}_n^f, \tilde{u}_r^f\right\}$ are the relative velocities before and after collision, $\tilde{\mathbf{p}}$ is the impulse expressed in the collision local coordinate system, and $\mathbf{L}$ defines the transformation from global to local coordinates, $\mathbf{L} = (\mathbf{t}, \mathbf{n}, \mathbf{r})^{\mathrm{T}}$. Because $\mathbf{L}$ is an orthogonal matrix, $\mathbf{L}^{-1} = \mathbf{L}^{\mathrm{T}}$.

The following sections present a brief overview of the methods proposed in the literature to compute impulse-based collision response.

Copyright © 2013 John Wiley & Sons, Ltd.

DOI: 10.1002/nme

2.1. Mirtich's collision matrix

Mirtich [6] proposed an approach to compute $\mathbf{p}$ using a collision matrix, which allows the computation of impulse at individual contact points as a function of relative velocity after collision. The derivation is shown here. Manipulating Equations (4) and (5), the change of linear velocity, $\triangle \mathbf{v}_i$, and angular velocity, $\triangle \boldsymbol{\omega}_i$, can be expressed as

$$\triangle \mathbf{v}_i = \frac{1}{m_i}\mathbf{p} \tag{13}$$

$$\triangle \boldsymbol{\omega}_i = \mathbf{I}_i^{-1}\mathbf{r}_i \times \mathbf{p} \tag{14}$$

which can be rewritten as [6]

$$\triangle \mathbf{u}_i = \left(\frac{1}{m_i}\mathbf{1} - \tilde{\mathbf{r}}_i \mathbf{I}_i^{-1}\tilde{\mathbf{r}}_i\right)\mathbf{p} \tag{15}$$

where $\triangle \mathbf{u}_i = \{\triangle u_i^x, \triangle u_i^y, \triangle u_i^z\}^{\mathrm{T}}$ and $\triangle \mathbf{u}_j = -\triangle \mathbf{u}_i$ are the change of velocities of body i and j at the contact point, and $\tilde{\mathbf{r}}_i$ is the cross-product matrix of $\mathbf{r}_i$, defined as

$$\tilde{\mathbf{r}} = \begin{pmatrix} 0 & -r^z & r^y \\ r^z & 0 & -r^x \\ -r^y & r^x & 0 \end{pmatrix} \tag{16}$$

By rewriting Equations (15) and (2), the change of relative velocity can be represented by a collision matrix, $\mathbf{K}$, as

$$\triangle \mathbf{u} = \mathbf{K}\mathbf{p} \tag{17}$$

$$\mathbf{K} = \left(\frac{1}{m_i} + \frac{1}{m_j}\right)\mathbf{1} - \left(\tilde{\mathbf{r}}_i \mathbf{I}_i^{-1}\tilde{\mathbf{r}}_i + \tilde{\mathbf{r}}_j \mathbf{I}_j^{-1}\tilde{\mathbf{r}}_j\right) \tag{18}$$

where $\mathbf{K}$ is constant, non-singular, symmetric, and positive definite [6], and $\mathbf{1}$ is the identity matrix. Thus, $\mathbf{p}$ is computed as

$$\mathbf{p} = \mathbf{K}^{-1}\triangle \mathbf{u} \tag{19}$$

where $\triangle \mathbf{u}$ is the change of relative velocity at the contact point.

2.1.1. Collision response without friction.

The empirical law for frictionless collisions assumes that the impulse is only applied in the direction normal to collision [49]. Thus, it models response by reversing the normal relative velocity

$$\tilde{u}_n^f = -e\tilde{u}_n^b \tag{20}$$

In Baraff's approach, the collision matrix is not used. Instead, by applying the previous constraint, the magnitude of the impulse is computed directly

$$|\mathbf{p}| = \frac{-\tilde{u}_n^b(e+1)}{\frac{1}{m_i} + \frac{1}{m_j} + \mathbf{n}^{\mathrm{T}}\left(\mathbf{I}_i^{-1}\left(\mathbf{r}_i \times \mathbf{n}\right)\right) \times \mathbf{r}_i + \mathbf{n}^{\mathrm{T}}\left(\mathbf{I}_j^{-1}\left(\mathbf{r}_j \times \mathbf{n}\right)\right) \times \mathbf{r}_j} \tag{21}$$

from which the impulse vector is given by $\mathbf{p} = |\mathbf{p}|\mathbf{n}$.

Copyright © 2013 John Wiley & Sons, Ltd.

DOI: 10.1002/nme

2.1.2. Collision response with friction, $\tilde{u}_n^f$ is not exactly inverse of $\tilde{u}_n^b$.
Hahn [34] introduced friction into the approach by assuming that the body is static after collision and neglecting the tangential velocity after collision

$$\mathbf{u}_f = -e\tilde{u}_n^b\mathbf{n} \tag{22}$$

which can be rewritten in local coordinates as

$$\begin{bmatrix} \tilde{u}_t^f & \tilde{u}_n^f & \tilde{u}_r^f \end{bmatrix}^T = \begin{bmatrix} 0 & -e\tilde{u}_n^b & 0 \end{bmatrix}^T \tag{23}$$

Once the relative velocity after collision is determined, if the static friction condition is satisfied,

$$|\mathbf{p}_t| < \mu|\mathbf{p}_n| \tag{24}$$

then $\mathbf{p}$ is computed using Equation (19), where μ is the coefficient of friction. If the static friction condition (24) is not satisfied, then, $\mathbf{p}$ is computed as follows:

$$\mathbf{p} = \mathbf{p}_n + \mu|\mathbf{p}_n|\mathbf{t}. \tag{25}$$

2.2. Collision response with friction, $\tilde{u}_n^f = -\tilde{u}_n^b$

Guendelman [7] proposed recomputing the impulse if the static friction assumption is not satisfied. Similarly to Baraff's impulse-based approach, it does so while constraining the relative velocity after collision to be exactly the inverse of the relative velocity before collision in the normal direction $\mathbf{n}$, $\tilde{u}_n^f = -\tilde{u}_n^b$. Then, the magnitude of impulse in the normal direction is computed using the collision matrix, $\mathbf{K}$, as follows:

$$|\mathbf{p}_n| = -\frac{\tilde{u}_n^b(e+1)}{\mathbf{n}^{\mathrm{T}}\mathbf{K}(\mathbf{n}-\mu\mathbf{t})} \tag{26}$$

When the static condition is not satisfied, the impulse is defined as

$$\mathbf{p} = |\mathbf{p}_n|\mathbf{n} + \mu|\mathbf{p}_n|\mathbf{t}. \tag{27}$$

3. ENERGY LOSS DURING COLLISION

Mirtich [6] proposed that the work carried out by contact forces, $\mathbf{W}$, during collision is path independent and is given by

$$\mathbf{W} = \frac{1}{2}\left(\mathbf{u}_b + \mathbf{u}_f\right)^{\mathrm{T}}\mathbf{K}^{-1}\left(\mathbf{u}_b - \mathbf{u}_f\right) \tag{28}$$

To ensure the conservation of energy of the entire system, this work should be zero. Mirtich [6] discussed the condition of energy conservation in the impulse-based method and proposed the following lemma:

Lemma 3.1
If during a collision the relative contact velocity is exactly reversed, that is to say, $\mathbf{u}_f = -\mathbf{u}_b$, then the work performed by the collision forces is zero, and the energy of the system is therefore unchanged by the collision.

Note that $\mathbf{u}_b = -\mathbf{u}_f$ is a potential solution that implies $\mathbf{W} = 0$. However, it neglects the change of velocity direction caused by the collision. For instance, after an object collides with the ground, the velocity in the normal direction should be reversed, whereas the velocity in the tangential direction should remain unchanged. Thus, this solution is not often chosen, despite the fact that it conserves energy.

An alternative condition for the energy conservative in the impulse-based method is now proposed.

Copyright © 2013 John Wiley & Sons, Ltd.

DOI: 10.1002/nme

Lemma 3.2
If the impulse is only applied in the normal direction and the relative velocity in the normal direction is exactly reversed, $\tilde{u}_n^f = -\tilde{u}_n^b$, then the energy of the system is conserved during collision.

Proof
By substituting Equation (19) into Equation (28), it is found that

$$\mathbf{W} = \frac{1}{2}(\mathbf{u}_b + \mathbf{u}_f)^{\mathrm{T}}\mathbf{p} \tag{29}$$

The work performed by the impulse can be expressed in terms of the defined local coordinate system, as follows:

$$\mathbf{W} = \frac{1}{2}(\mathbf{L}^{-1}\tilde{\mathbf{u}}_f + \mathbf{L}^{-1}\tilde{\mathbf{u}}_b)^{\mathrm{T}}(\mathbf{L}^{-1}\tilde{\mathbf{p}}) \tag{30}$$

$$\mathbf{W} = \frac{1}{2}(\tilde{\mathbf{u}}_f + \tilde{\mathbf{u}}_b)^{\mathrm{T}}\left(\mathbf{L}^{-1}\right)^{\mathrm{T}}\left(\mathbf{L}^{-1}\right)\tilde{\mathbf{p}} \tag{31}$$

where $(\mathbf{L}^{-1})^{\mathrm{T}}\mathbf{L}^{-1} = \mathbf{1}$, and so,

$$\mathbf{W} = \frac{1}{2}\left(\tilde{\mathbf{u}}_f + \tilde{\mathbf{u}}_b\right)^{\mathrm{T}}\tilde{\mathbf{p}} = \frac{1}{2}\left[\tilde{u}_t^f + \tilde{u}_t^b, \tilde{u}_n^f + \tilde{u}_n^b, \tilde{u}_r^f + \tilde{u}_r^b\right]\begin{bmatrix}\tilde{p}_t \\ \tilde{p}_n \\ \tilde{p}_r\end{bmatrix} = 0 \tag{32}$$

It assumes that $\tilde{u}_n^f = -\tilde{u}_n^b$, and the impulse is only applied to the normal direction. Thus, $\tilde{p}_t = 0$ and $\tilde{p}_r = 0$, and so

$$\mathbf{W} = \frac{1}{2}\left[\tilde{u}_t^f + \tilde{u}_t^b, 0, \tilde{u}_r^f + \tilde{u}_r^b\right]\begin{bmatrix}0 \\ \tilde{p}_n \\ 0\end{bmatrix} = 0 \tag{33}$$

□

Lemma 3.2 defines a necessary condition for the impulse-based method to model an energy conservative collision, implying that there should be no energy loss during impact, and that no artificial source or sink of energy is introduced by the numerical method. The energy conservative collision is ideal, in that no friction or other energy loss sources are taken into account. However, the ability to simulate frictionless and perfectly elastic collisions remains a basic requirement for realistic impact mechanics simulation. Approaches proposed by Baraff [4] and Guendelman [7] both satisfy this lemma, indicating that they are energy conservative, whereas the approach proposed by Hahn [34] does not.

4. NUMERICAL TESTS

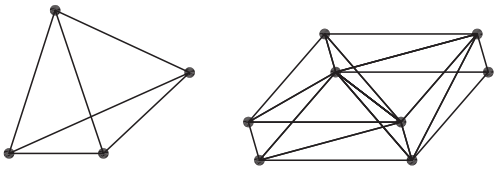
Numerical tests are now used to investigate energy and linear momentum conservation of the approaches proposed by Hahn [34] and Guendelman [7]. In all tests, density is 1 kg/m^3 and the default time step is 1/600 s. The ability to capture energy conservation and linear momentum conservation is essential for a numerical method to simulate collisions correctly. The total system energy, E, is expressed as

$$E = \sum_i^n \left(E_i^p + E_i^k\right) = \sum_i^N \left(m_i g h_i + \int_{V_i} \frac{\mathbf{u}^2(\mathbf{x})}{2}\mathrm{d}m\right) \tag{34}$$

where n is the number of bodies, E_i^p and E_i^k are the potential energy and kinetic energy of body i, m_i is the mass of body i, g is gravity acceleration, h_i is the height of the center of gravity of body

Copyright © 2013 John Wiley & Sons, Ltd.

DOI: 10.1002/nme



(a) (b)

Figure 2. Geometric representation of bodies.

i, V_i is the volume, and $\mathbf{u}(\mathbf{x})$ is the linear velocity at integration point $\mathbf{x}$. The system is expected to be energy conservative for the special case of perfectly elastic collisions, where $\mu = 0$ and $e = 1$. For the case of perfectly elastic collisions, the relative error of E is measured as follows:

$$\varepsilon_e = \left| \frac{E^b - E^f}{E^b} \right| \tag{35}$$

where E^b and E^f are the energies before and after collision, and ε_e is the relative error of energy. The total linear momentum of the system is computed as

$$\mathbf{M} = \sum_i^n m_i \mathbf{v}_i \tag{36}$$

where $\mathbf{M} = \{M_x, M_y, M_z\}^{\mathrm{T}}$. If there is no external force acting on a closed system, the linear momentum of the system remains constant. The relative error in the linear momentum of a closed system is defined as

$$\varepsilon_M = \max\left(\left| \frac{M_x^f - M_x^b}{M_x^b} \right|, \left| \frac{M_y^f - M_y^b}{M_y^b} \right|, \left| \frac{M_z^f - M_z^b}{M_z^b} \right| \right) \tag{37}$$

where $\mathbf{M}^b$ and $\mathbf{M}^f$ refer to the linear momenta before and after collision. Throughout the aforementioned discussion, it is known that IM-Guendelman is able to capture the property of energy conservation, because it is able to ensure that $\tilde{u}_n^f = -\tilde{u}_n^b$. However, IM-Hahn is not able to capture the property of energy conservation, because $\tilde{u}_n^f$ is not exactly the inverse of $\tilde{u}_n^b$. In the following, several numerical tests are simulated using IM-Guendelman and IM-Hahn, respectively, and the energy and linear momentum before and after collision are measured and compared. These tests include collision of two tetrahedral fragments, a sphere falling down a slope, and ore fragments flowing through a cylindrical draw point in a block-cave mine [50].

In these tests, each body, convex or non-convex, is represented by a conglomerate of tetrahedra (Figure 2).

4.1. Collision of two tetrahedra

The energy momentum and linear momentum conservative properties of the collision of two tetrahedra are measured in this test (see Figure 3(a,b)). To eliminate the numerical error from the computation of velocity change caused by gravity, it is assumed that $g = 0$ m/s^2. In the first part of the test, (1) body j is fixed and static, whereas another, body i, moves with an initial velocity and eventually collides with it (Figure 3). In test (b), body j is initially static but moves after the collision. In test (a), the initial linear velocity is $\mathbf{v}_1 = (0, 0, -10)$ m/s, and the initial angular velocity is $\boldsymbol{\omega}_1 = (0, 0, -10)$ m/s. In test (b), initial linear velocities are $\mathbf{v}_1 = (0, 0, -10)$ m/s and $\mathbf{v}_2 = (0, 0, 0)$ m/s, and initial angular velocities are $\boldsymbol{\omega}_1 = (5, 10, 3)$ m/s and $\boldsymbol{\omega}_2 = (0, 0, 0)$ m/s.

Figure 3(b) shows snapshots of the simulation. In (b), no external force acts on the two tetrahedra. Therefore, this is a closed system. Results, shown in Table I, suggest that both IM-Hahn and IM-

Copyright © 2013 John Wiley & Sons, Ltd.

DOI: 10.1002/nme

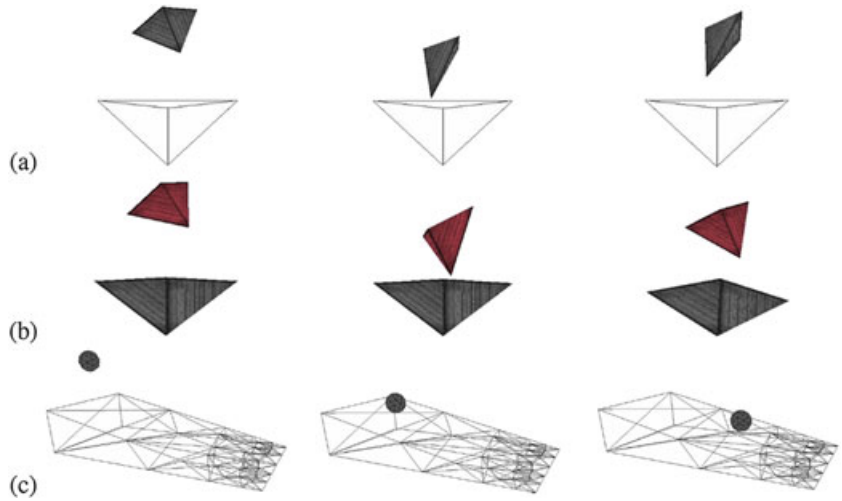


Figure 3. Moving tetrahedra colliding with (a) one static tetrahedron, (b) a moving tetrahedron, and (c) images of a spherical object falling down a slope. Wireframe rendering denotes static bodies. In (a) and (b), objects are defined as tetrahedron 1, node list: (−1, 1, 0), (1, 1, 0), (1, −1, 0), (1, 1, −2); tetrahedron 2, node list: (−2, 2, −4), (2, 2, −4), (2, −2, −4), (2, 2, −6).

Table I. Energy and linear momentum for (a) a moving tetrahedron collides with a static one; (b) two colliding tetrahedra.

	(a) IM-Hahn	(a) IM-Guendelman	(b) IM-Hahn		(b) IM-Guendelman	
Timestep size	ε_e	ε_e	ε_e	ε_m	ε_e	ε_m
1/60	−2.1192	4.37×10^{-8}	-2.11×10^{-2}	0.00	5.91×10^{-4}	0.00
1/120	−2.1192	-4.15×10^{-9}	-2.11×10^{-2}	0.00	5.91×10^{-4}	0.00
1/300	−2.1906	-1.18×10^{-9}	-2.57×10^{-2}	0.00	7.48×10^{-4}	0.00
1/600	−2.1906	-4.06×10^{-8}	-2.57×10^{-2}	0.00	7.48×10^{-4}	0.00
1/900	−2.1906	3.71×10^{-8}	-2.57×10^{-2}	0.00	7.48×10^{-4}	0.00
1/1200	−2.1906	-9.06×10^{-9}	-2.63×10^{-2}	0.00	7.65×10^{-4}	0.00
1/2400	−2.2027	1.44×10^{-8}	-2.63×10^{-2}	0.00	7.65×10^{-4}	0.00

Guendelman are linear momentum conservative. However, IM-Guendelman appears to be energy conservative, whereas IM-Hahn does not.

4.2. Sphere falling down a slope

The movement of a sphere bouncing down a fixed slope is now investigated (Figure 3(c)). The diameter of the sphere is $d = 2$ m, at an initial height of $h = 4$ m, and the slope is $a : b = 1 : 10$ (Figure 4(a)). In the following tests, $g = 9.81$ m/s^2. The sphere is a conglomerate of 106 tetrahedra, whereas the slope is represented by 115 tetrahedra. Perfectly, elastic collisions are considered. The energy change during the simulation is shown in Figure 4(b). When IM-Guendelman is used, the average relative error is 2.28×10^{-5}. However, for the IM-Hahn, a relative error in the energy of up to 0.45 is found.

4.3. Draw point

Block caving is a methodology to extract massive ore fragments from underground mines in which ore fragments collapse because of gravity and are collected through an undercutting draw point [50]. The gravity-driven fall of 490 ore fragments through a single draw point in a block-cave mine is modeled. The heap width is taken to be $a = 20$ m. The draw point is a cylinder of radius $r = 5.6$ m

Copyright © 2013 John Wiley & Sons, Ltd.

DOI: 10.1002/nme

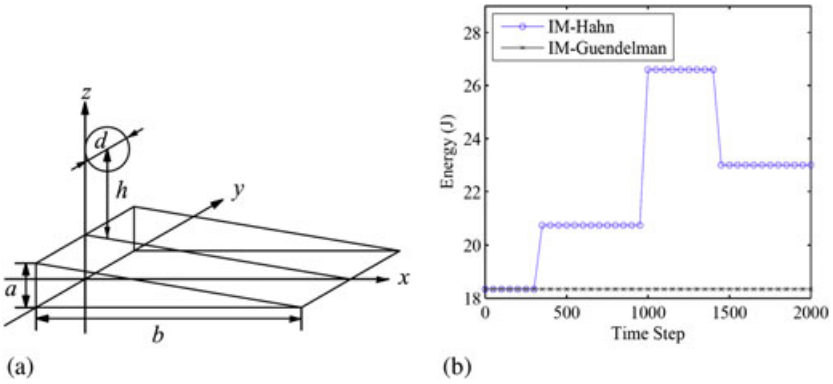


Figure 4. (a) Details of the slope test. (b) Energy change of a sphere bouncing down a slope.

and depth $c = 11.6$ m, and the thickness of the wall is $d = 5$ m. The radii of ore particles is approximately 3 m, and the initial height of the heap is $b \approx 45$ m. To simplify the simulation model, only a quarter of the model is considered, as shown in Figure 5 (a). Each ore particle has the same shape and contains 16 tetrahedra. Figure 6 shows the initial and final stages of the system, for $e = 0.8$ and $\mu = 0.5$. Energy values as a function of simulation progression are shown in Figure 5(b) for different friction and restitution values and in more detail, in Figure 5(c) for the perfectly elastic case. It is observed that the energy discrepancy increases when IM-Hahn is used. Results suggest that for $e = 1, \mu = 0$ energy is conservative, with a relative error of less than 1×10^{-3}. For $e \neq 1, \mu \neq 0$, the energy of the system decreases accordingly.

5. CONCLUDING REMARKS

In the present work, the energy conservative property and momentum conservative property of the impulse-based collision method have been discussed. A necessary condition for the impulse-based method to be energy conservative was proposed. According to the condition, Guendelman's impulse-based approach is energy conservative, whereas Hahn's approach does not appear to. Both approaches are investigated numerically in terms of energy and momentum conservations. Both approaches appear to conserve linear momentum. The impulse method conserves energy and was shown to be a stable and fast method for collision resolution in a system of non-convex polyhedral objects.

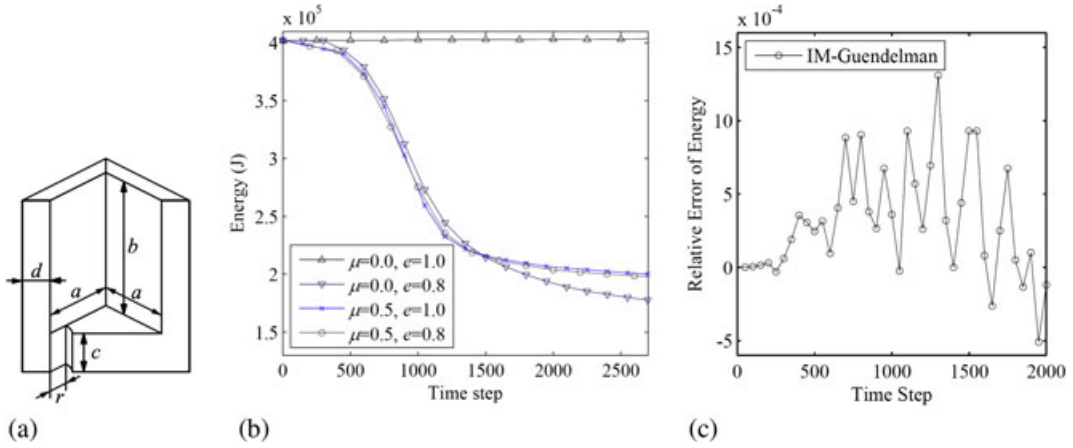


Figure 5. (a) Details of the single draw point test. (b) Energy curve for the system of fragments falling through a cylindrical draw point with different friction and restitution values. (c) Relative error of total energy for the case of perfectly elastic collisions.

Copyright © 2013 John Wiley & Sons, Ltd.

DOI: 10.1002/nme

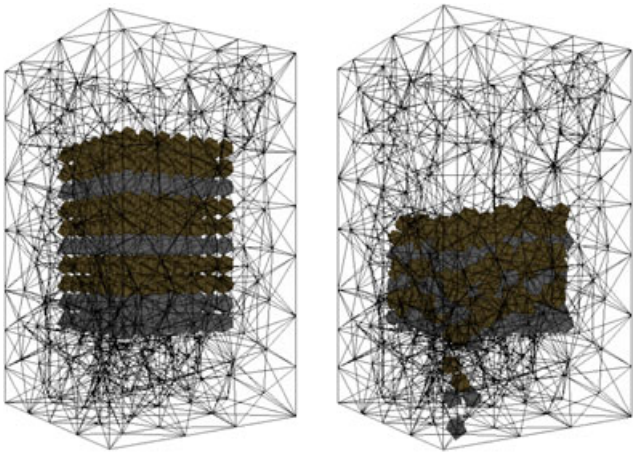


Figure 6. Collision of $7 \times 7 \times 10 = 490$ ores, around a single draw point, at (a) initial and (b) intermediate stages. Fragments stop falling through the draw point after $\approx$ 12k iterations. Bodies are conglomerates comprising 9208 tetrahedra.

ACKNOWLEDGEMENTS

The authors would like to thank Rio Tinto for supporting this work, through the Rio Tinto Centre for Advanced Mineral Recovery at Imperial College.

REFERENCES

1. Vyazmensky A. Numerical modeling of surface subsidence associated with block cave mining using a finite element / discrete element approach. *PhD Thesis*, Simon Fraser University, Burnaby, Canada, 2008.
2. Munjiza A, Latham J. Comparison of experimental and FEM/DEM results for gravitational deposition of identical cubes. *Engineering Computations* 2004; **21**(2-3):249–264.
3. Mishra BA. Review of computer simulation of tumbling mills by the discrete element method: Part II: practical applications. *International Journal of Mineral Processing* 2003; **71**(1-4):95–112.
4. Baraff D. Fast contact force computation for nonpenetrating rigid bodies. *Computer Graphics* 1994; **28**:23–34.
5. Guises R, Latham JP, Munjiza A. Granular packing: numerical simulation and the characterisation of the effect of particle shape. *Granular Matter* 2009; **11**(5):281–292.
6. Mirtich B. Impulse-based dynamic simulation of rigid body systems. *PhD Thesis*, University of California, Berkeley, 1996.
7. Guendelman E, Bridson R, Fedkiw R. Nonconvex rigid bodies with staking. *ACM Transaction on Graphics* 2003; **22**(3):871–878.
8. Belytschko T. The splitting pinball method for contact-impact problems. *Computer Methods in Applied Mechanics and Engineering* 1993; **105**(3):375–393.
9. Babuska I. The finite element method with penalty. *Mathematics of Computation* 1973; **27**(122):221–228.
10. Bourago N, Kukudzhanov VN. A review of contact algorithms. *The Institute for Problems in Mechanics of RAS, Moscow, lzv. RAN. MTT* 2005; **1**:45–87.
11. Hasegawa S. Real-time rigid body simulation based on volumetric penalty method. *11th Symposium on Haptic Interfaces for Virtual Environment and Teleoperator Systems*, Los Angeles, CA, USA, 2003; 326–332.
12. Wang Y, Tonon F. Discrete element modeling of rock fragmentation upon impact in rock fall analysis. *Rock Mechanics and Rock Engineering* 2011; **44**:23–35.
13. Hentz S, Daudeville L, Donzé F. Identification and validation of a discrete element model for concrete. *Journal of Engineering Mechanics, ASCE* 2004; **130**:709–719.
14. McCarthy J, Jasti V, Marinack M, Higgs C. Quantitative validation of the discrete element method using an annular shear cell. *Powder Technology* 2010; **203**:70–77.
15. Laursen T, Chawla V. Design of energy conserving algorithms for frictionless dynamic contact problems. *International Journal for Numerical Methods in Engineering* 1997; **40**(5):863–886.
16. Drumwright E. A fast and stable penalty method for rigid body simulation. *IEEE Transactions on Visualization and Computer Graphics* 2008; **14**(1):231–240.
17. Haikal G, Hjelmstad KD. A finite element formulation of non-smooth contact based on oriented volumes for quadrilateral and hexahedral elements. *Computer Methods in Applied Mechanics and Engineering* 2007; **196**:4690–4711.

Copyright © 2013 John Wiley & Sons, Ltd.

DOI: 10.1002/nme

18. Noels L, Stainier L, Ponthot J. An energy momentum conserving algorithm using the variational formulation of visco-plastic updates. *International Journal for Numerical Methods in Engineering* 2006; **65**(6):904–942.
19. Chawla V, Laursen T. Energy consistent algorithms for frictional contact problems. *International Journal for Numerical Methods in Engineering* 1998; **42**(5):799–827.
20. Munjiza A, Andrews K. Penalty function method for combined finite-discrete element systems comprising large number of separate bodies. *International Journal for Numerical Methods in Engineering* 2000; **49**:1377–1396.
21. Cundall PA, Strack ODL. A discrete numerical model for granular assemblies. *Geotechnique* 1979; **29**:47–65.
22. Magnier S, Donz F. Numerical simulations of impacts using a discrete element method. *Mechanics of Cohesive-frictional Materials* 1999; **3**(3):257–276.
23. Lucy LB. A numerical approach to the testing of the fission thesis. *Astronomical Journal* 1977; **82**:1013–1024.
24. R G JM. Smoothed particle hydrodynamics theory and application to non-spherical stars. *Monthly Notices of the Royal Astronomical Society* 1977; **181**:375–389.
25. Shi G, Goodman R. Discontinuous deformation analysis. *The 25th U.S. Symposium on Rock Mechanics (USRMS), June 25-27*, Evanston, IL, 1984; 269–278.
26. Latham L, Munjiza A, Garcia X, Xiang J, Guisesa R. Three-dimensional particle shape acquisition and use of shape library for DEM and FEM/DEM simulation. *Minerals Engineering* 2008; **21**:797–805.
27. Latham J, Munjiza A, Mindel J, Xiang J, Guises R, Garcia X, Pain C, Gorman G, Piggott M. Modelling of massive particulates for breakwater engineering using coupled FEMDEM and CFD. *Particuology* 2008; **6**(6):572–583.
28. Chandramohan R, Powell M. Measurement of particle interaction properties for incorporation in the discrete element method simulation. *Minerals Engineering* 2005; **18**(12):1142–1151.
29. Liu G, Liu M. *Smooth Particle Hydrodynamics: A Meshfree Particle Method*. World Scientific: Singapore, 2003.
30. Bardenhagen S, Brackbill J, Sulsky D. The material-point method for granular materials. *Computer Methods in Applied Mechanics and Engineering* 2000; **187**(3-4):529–541.
31. Sulsky D, Kaul A. Implicit dynamics in the material-point method. *Computer Methods in Applied Mechanics and Engineering* 2004; **193**(12-14):1137–1170.
32. Campbell J, Vignjevic R, Libersky L. Computer methods in applied mechanics and engineering. *Computer Methods in Applied Mechanics and Engineering* 2000; **184**(1):49–65.
33. Chardonnet J, Miossec S, Kheddar A, Arisumi H, Hirukawa H, Pierrot F, Yokoi K. Dynamic simulator for humanoids using constraint-based method with static friction. *Proceedings of IEEE International Conference on Robotics and Biomimetics*, Kunming, China, 2006; 1366–1371.
34. Hahn JK. Realistic animation of rigid bodies. *Computer Graphics* 1988; **22**(4):299–308.
35. Schmitt A, Bender J, Prautzsch H. On the convergence and correctness of impulse-based dynamic simulation. *Internal Report 17*, Institut für Betriebs- und Dialogsysteme, Fakultät für Informatik, Karlsruhe Univeristy, Karlsruhe, Germany, 2005.
36. Mirtich B, Canny J. Impulse-based simulation of rigid bodies. *Proceedings of the 1995 symposium on interactive 3D graphics*, New York, USA, 1995; 181–188.
37. Lin M. Efficient collision detection for animation and robotics. *PhD Thesis*, University of California, Berkeley, 1993.
38. Lin M, Canny J. A fast algorithm for incremental distance calculation. *Proceeding of the IEEE International Conference on Robotics and Automation*, IEEE, Sacramento, CA, USA, 1991; 1008–1014.
39. Paluszny A, Tang X, Zimmerman R. A multi-modal approach to 3D fracture and fragmentation of rock using impulse-based dynamics and the finite element method. *The 46th US Rock Mechanics/Geomechanics Symposium*, Chicago, IL, USA, 2012; 24–27.
40. Wang Y, Tonon F. Calibration of a discrete element model for intact rock up to its peak strength. *International Journal for Numerical and Analytical Methods in Geomechanics* 2010; **34**(5):447–469.
41. Ma S, Zhang X, Qiu X. Comparison study of MPM and SPH in modeling hypervelocity impact problems. *International Journal of Impact Engineering* 2009; **36**(2):272–282.
42. Powell M, McBride A. What is required from DEM simulations to model breakage in mills? *Minerals Engineering* 2006; **19**(10):1013–1021.
43. Khanal M, Powell M. Energy representation for the unified comminution model. *Particulate Science and Technology: An International Journal* 2010; **28**(6):529–538.
44. Powell M, Govender I, McBride A. Applying DEM outputs to the unified comminution model. *Minerals Engineering* 2008; **21**:744–750.
45. Garstenauer H. A unified framework for rigid body dynamics. *PhD Thesis*, Johannes Kepler Universitaet, Linz, Austria, 2006.
46. Schiehlen W, Valasek M. *Virtual Nonlinear Multibody Systems*. Kluwer Academic Publishers: The Netherlands, 2002.
47. Hunt K, Grossley F. Coefficient of restitution interpreted as damping in vibroimpact. *Journal of Applied Mechanics* 1975; **42**(2):440–445.
48. Tonon F. Explicit exact formulas for the 3-D tetrahedron inertia tensor in terms of its vertex coordinates. *Journal of Mathematics and Statistics* 2004; **1**:8–10.
49. Baraff D. An introduction to physically based modeling: rigid body simulation II - nonpenetration constraints. *Technical Report*, Robotics Institute, Carnegie Mellon University, Pittsburgh, USA, 1997.
50. Brown E. *Block Caving Geomechanics*. Julius Kruttschnitt Mineral Research Centre, University of Queensland: Brisbane, Australia, 2003.

Copyright © 2013 John Wiley & Sons, Ltd.

DOI: 10.1002/nme